Some Remarks on Finite Element Modeling of Electromigration in Solder Joints

P. Dandu[1], X.J. Fan[1,*], Y. Liu[2]
[1]Department of Mechanical Engineering
Lamar University
PO Box 10028, Beaumont, TX 77710, USA
[2]Fairchild Semiconductor Corp.,
82 Running Hill Rd, South Portland, ME 04106, USA
xuejun.fan@lamar.edu

Abstract

This paper investigates several issues in finite element modeling of electromigration in solder joints: current density and thermal stress singularities; negative divergences of atomic fluxes due to electron current and thermal stresses; and submodeling accuracy. A copper post wafer level package is used as a test vehicle for simulation. Coupled electrical-, thermal-, and mechanical finite element modeling is performed. Results show that the values of maximum current density in solder balls significantly depend on finite element mesh sizes, indicating a singularity exists. Negative values of the divergences of atomic fluxes due to electron current and thermal stresses are obtained under certain loading conditions. Submodeling presents accurate results if cut boundary is appropriately chosen.

1. Introduction

The electromigration of solder joints under high current density is of reliability concern in wafer level packaging (WLP). Voids nucleation near cathode side and hillock development near anode side during current stressing indicates a biased mass diffusion from cathode to anode, which is referred to as electromigration (EM). The EM damage mechanism in solder balls is distinctly different from that in Al or Cu interconnects. For interconnects, EM damage is induced by the mass transport of only one type of atoms (Al or Cu) driven by electron wind. For solder alloys, intermetallic compounds (IMCs) are formed as a result of solid state reaction between solder and Cu or under bump metallurgy (UBM) [1]. Cu or Ni is fast diffusing species in Pb or Sn. At the device operating temperature above 100°C, the diffusivity of Cu in Pb or Sn is greater than the self-diffusivity of Pb or Sn. Consequently, several mechanisms are present during current stressing in solder joints. Electron wind can drive the predominant diffusion species from cathode side to anode side, causing void nucleation and growth between the IMC and solder alloy. At the same time, IMC reaction induced Sn consumption can generate more vacancies and therefore accelerate void nucleation [2]. Electromigration behavior of solder materials in electronic packaging is very complicated as compared to Al and Cu interconnects [3].

It is generally accepted that, in addition to the electromigration due to electron wind, temperature gradient induced thermal migration (TM) and thermo-mechanical stress (hydrostatic stress) gradient induced stress migration (SM) also play an important role in EM failures during current stressing. Tan et al. [4] performed a coupled-field finite element modeling for Cu interconnects, and found that the SM may be a dominant driving force for Cu narrow interconnect failures. Ye et al. [5] conducted electromigration test for flip chip solder joints, and observed the void formation on the anode side of solder joints near silicon chip. Electromigration alone could not explain this observation. Such failures are attributed to the thermal induced migration.

Dalleau et al. [6] developed an algorithm for three-dimensional finite element simulation of void formation in metallization, in which the EM, TM and SM are taken into considerations. However, singularity problems were not addressed. Liu et al. [7] adopted a similar methodology to investigate the electromigration due to EM, TM and SM in solder joints for both SnPb and SnAgCu alloys. From the results of finite element simulations, both TM and SM make contributions to the electromigration failures.

In finite element stress analysis, it has been understood that the stress singularity occurs at the edge of bimaterial (or multi-material) interface, crack tip, or wedge tip [8]. A preliminary work of finite element modeling of electromigration in solder joints by the authors found a mesh-size dependency of current density distribution in wafer level packages [9].

In this paper, some issues in finite element modeling of electromigration in solder joints are addressed. A copper post wafer level package is used as a test vehicle for simulation. Three-dimensional (3D) coupled electrical-thermal-mechanical finite element analysis is performed. The following problems are investigated: (1) effect of singularity of current density; 2) negative divergences of atomic fluxes due to EM and SM; and 3) the accuracy of submodeling approach used in electromigration modeling.

2. Background Theory

The coupled thermal-electrical governing equations can be expressed as follows [9],

$$\nabla \cdot \left(\frac{\nabla V}{\rho}\right) = 0 \tag{1}$$

$$\nabla \cdot (k\nabla T) + \frac{1}{\rho}|\nabla V|^2 = 0 \tag{2}$$

where T is temperature, V is the electrical potential, k is thermal conductivity, and ρ is the electric resistivity, which is a function of temperature as follows

$$\rho = \rho_0\left(1 + \alpha(T - T_0)\right) \tag{3}$$

α is thermal coefficient of resistivity, and ρ_0 and T_0 are initial constants. The joule heating is expressed by the second term on the left side in Equation (2). The above equations can be solved with the appropriate boundary conditions. Steady-state temperature distribution is assumed. The relationship between current density vector $\vec{j}$ and the electrical potential V is as follows:

$$\vec{J} = -\frac{\nabla V}{\rho} \quad (4)$$

After the electrical and temperature fields are solved, a sequentially coupled thermal stress analysis can be performed to obtain the thermo-mechanical stress distribution. The mismatch in the coefficient of thermal expansion (CTE) in different materials present in the system leads to development of the thermal stress fields.

The degradation of metallization structures is due to the presence of atomic flux divergence caused by electrical, thermal and stress induced mass transport. The mathematical expressions defining the atomic fluxes due to electromigration, thermo-migration and stress-migration are as follows [6]:

$$\vec{J}_{Em} = \frac{N}{K_B T} eZ^* \rho D_0 \exp\left(-\frac{E_A}{K_B T}\right)\vec{J} \quad (5)$$

$$\vec{J}_{Th} = -\frac{NQ^* D_0}{K_B T^2} \exp\left(-\frac{E_A}{K_B T}\right)\nabla T \quad (6)$$

$$\vec{J}_s = -\frac{N\Omega D_0}{K_B T} \exp\left(-\frac{E_A}{K_B T}\right)\nabla \sigma_H \quad (7)$$

where,

N is the atomic concentration,
e is the electron charge,
$\vec{J}$ corresponds to the local current density vector,
D_0 is the self diffusion coefficient,
K_B is the Boltzmann constant,
T is the value of the local temperature,
Z^* represents the effective charge of ions,
Ω is the atomic volume,
Q^* is the specific heat of transport,
E_A is the activation energy of the material,
σ_H is the local hydrostatic stress value
$\sigma_H = (\sigma_{xx} + \sigma_{yy} + \sigma_{zz})/3)$, where σ_{xx}, σ_{yy}, and σ_{zz} correspond respectively to the normal components provided by the local stress tensor.

The local atomic concentration of diffusion species is related to the atomic fluxes by the equation as follows,

$$\mathrm{div}(\vec{J}_{Em} + \vec{J}_{Th} + \vec{J}_s + \vec{J}_N) + \frac{\partial N}{\partial t} = 0 \quad (8)$$

where $\vec{J}_N = -D_0 \exp\left(-\frac{E_A}{K_B T}\right)\nabla N$. The individual atomic flux divergence because of electromigration, thermo-migration, and stress-migration are derived as following [6]:

$$\mathrm{div}(\vec{J}_{Em}) = \left(\frac{E_A}{K_B T^2} - \frac{1}{T} + \alpha\frac{\rho_0}{\rho}\right)\vec{J}_{Em} \cdot \nabla T \quad (9)$$

$$\mathrm{div}(\vec{J}_{Th}) = \left(\frac{E_A}{K_B T^2} - \frac{3}{T} + \alpha\frac{\rho_0}{\rho}\right)\vec{J}_{Th} \cdot \nabla T + \frac{NQ^* D_0}{3{K_B}^3 T^3} j^2 \rho^2 e^2 \exp\left(-\frac{E_A}{K_B T}\right) \quad (10)$$

$$\mathrm{div}(\vec{J}_s) = \left(\frac{E_A}{K_B T^2} - \frac{1}{T}\right)\vec{J}_s \cdot \nabla T - \frac{2N\Omega D_0 E\alpha_l}{3K_B T(1-v)} \exp\left(-\frac{E_A}{K_B T}\right)\left\{\frac{j^2\rho^2 e^2}{3{k_B}^2 T} + \left(\frac{1}{T} - \alpha\frac{\rho_0}{\rho}\right)\nabla^2 T\right\} \quad (11)$$

where E is Young modulus, v is the poisson ratio, α_l coefficient of thermal expansion, α is the thermal coefficient of resistivity. In deriving the above expressions, the gradient of the atomic concentration ∇N is neglected. Therefore, the divergence due to self-diffusion is zero. The total divergence of atomic flux is now defined as:

$$\mathrm{div}(\vec{J}_{Tot}) = \mathrm{div}(\vec{J}_{Em}) + \mathrm{div}(\vec{J}_{Th}) + \mathrm{div}(\vec{J}_s) \quad (12)$$

3. Finite Element Models

The package chosen for the analysis is a copper post wafer level package, which has a 6×6 solder ball array with 0.5×0.5mm ball pitch. The exterior 20 balls are electrically connected with each other in a daisy chain format. Because of the symmetry of the package (Figure 1(a)), a quarter-model is constructed, as shown in Figure 1(b). Submodeling approach is applied. In the global model, all solder balls can be simplified as rectangular blocks. However, in the present global model, the corner solder ball of the interest is of the actual ball shape with all details of ball structure as shown in Figure 1(b) & (c), since the refined global model will be used in the subsequent analysis to verify the submodeling accuracy (see Section 6). In the submodel (Figure 1(d)), three electrically connected bumps are selected, two of which are simplified as rectangular blocks (Figure 1(e)). It is a known fact that the EM failure in solder bumps occurs on cathode side near interface. So the finite element mesh for the corner solder bump is designed with a dense meshing along the interface as shown in Figure 1(f). The cut boundary through PCB should have sufficient distance to the ball to ensure the accuracy of submodeling (to be discussed in Section 6).

The following boundary conditions are applied: on one end of the electrical connection, the voltage potential is set grounded (zero), while the other end is given as a lumped current load of ±1.7A [7]. The ambient temperature surrounding the test structure is 50°C, and the convective heat transfer coefficient is 20 W/m^2°C.

SOLID5 8-node 3D element in ANSYS 11.0 is used. SOILD5 can perform coupled electrical-, thermal-, and stress modeling. The epoxy, silicon chip and PCB in this model do not conduct electricity, thus very high resistance values are assigned to these materials. The electromigration parameters used in calculating the atomic fluxes by Equations 5-11 for SnAgCu solder bump are listed in Table 1 [10-16].

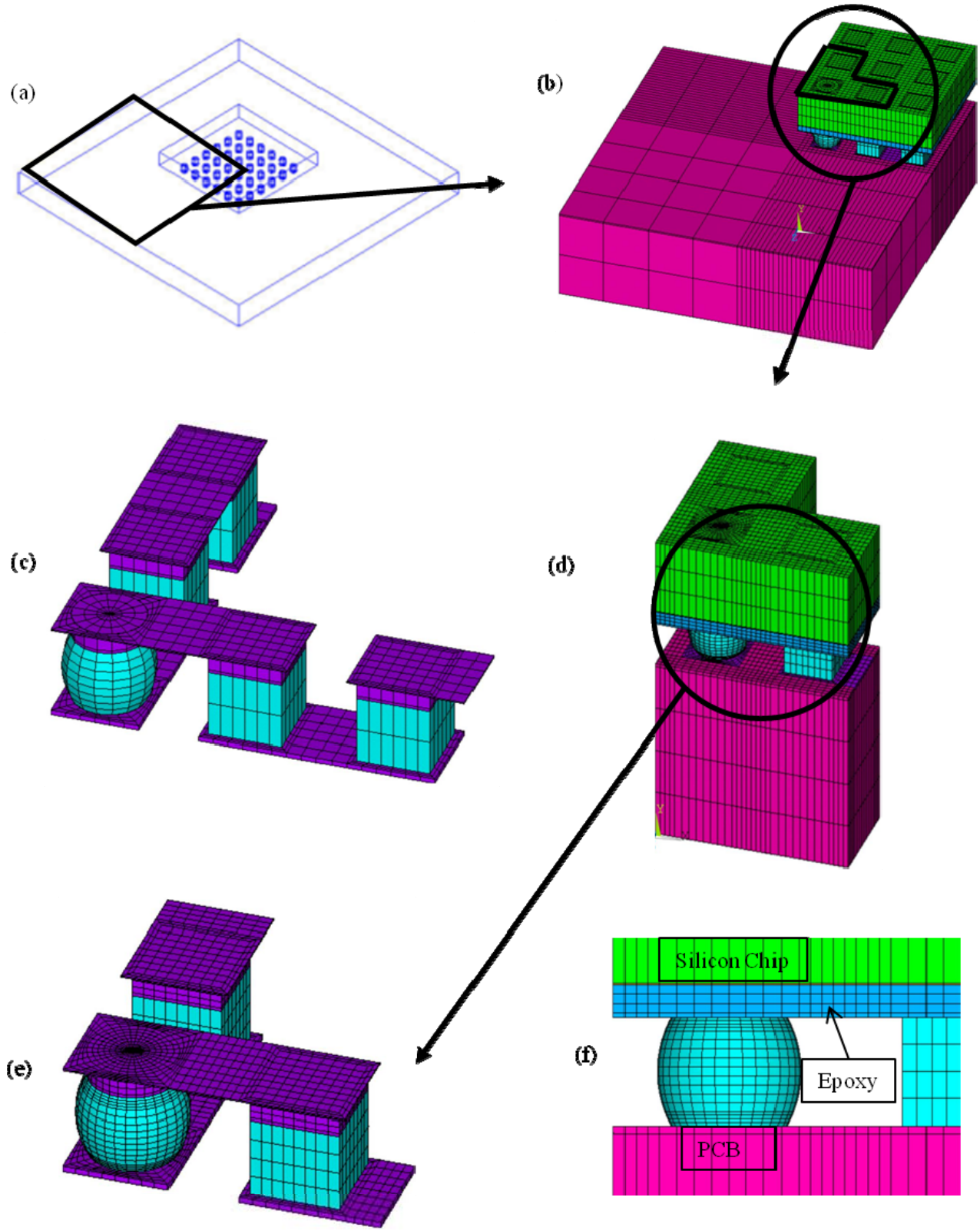

Figure 1 Global and local models **(a)** a WLP package **(b)** global model **(c)** electrical connectivity in global model **(d)** submodel mesh **(e)** electrical connectivity in submodel **(f)** front view of submodel showing detailed mesh pattern of the corner ball

Table 1 Basic Electromigration Parameters

Parameter	Units	Value
E_A	eV	0.8
Z^*	-	-23
D_0	m^2/s	0.027
Q^*	eV	0.0094
ρ_0	Ω·m	13.3e-8
α	1/K	2.8e-3
Ω	m^3/atom	2.72e-29
K_B	-	1.38066e-23
e	-	1.60219E-19

4. Effect of Singularity

To investigate the effect of singularity, three different mesh schemes are considered in the submodel for the corner ball. Figure 2 shows three mesh patterns, denoted by 'X', 'X/2' and 'X/4', indicating the mesh size is reduced by a factor of two each time.

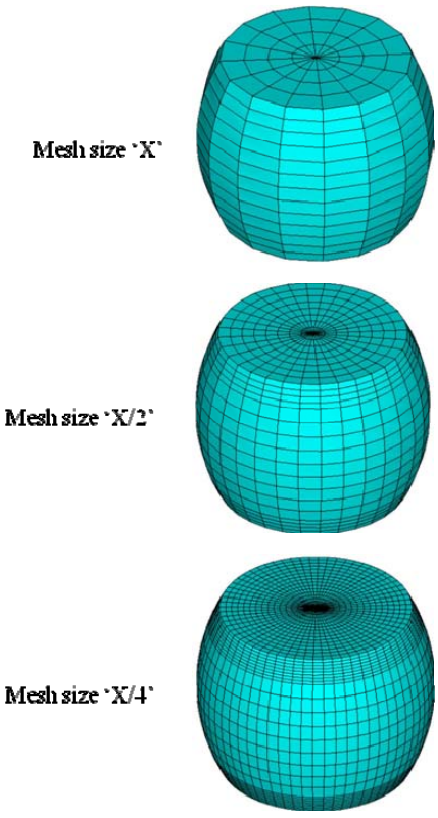

Figure 2 Three different mesh schemes

In this analysis, the electrons flow through the corner ball from PCB to silicon chip, thus the electromigration is expected to be on PCB side. The current density and stress distribution in the solder ball near PCB side are examined. Figure 3 shows the contours of the current density with three different meshes. The current density contour plot presented in this paper is the sum of three components of the current density vector. Cleary it shows the strong dependency with mesh size. As the mesh size is reduced by a factor of four, the maximum current density value is almost doubled.

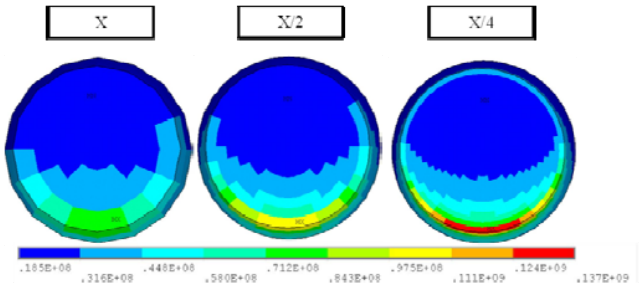

Figure 3 Current density contour with different meshes in corner ball (bottom view)

Figure 4 shows the contours of hydrostatic stress with three different meshes. The maximum stress also increases from 76MPa to 168MPa when the mesh size is reduced by a factor four.

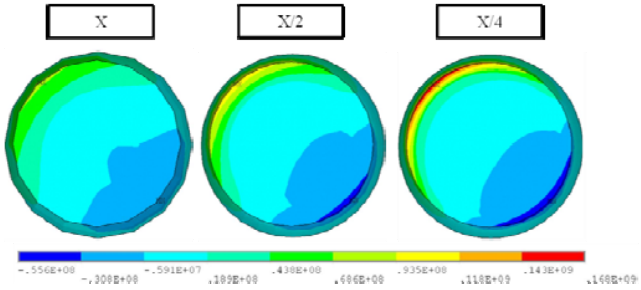

Figure 4 Hydrostatic stress contour with different meshes in corner ball (bottom view)

Table 2 summarizes the results of the maximum current density, temperature and hydrostatic stress. Unlike stress and current density, temperature doesn't display a singularity. A very consistent result is obtained for temperature for all three meshes.

Table 2 Variation of Max. Current Density, Max. Temperatures and Max. Hydrostatic Stresses with Different Mesh Sizes

Mesh size	Max. Current densities (A/m^2)	Max. Temperatures (K)	Max. Hydrostatic stresses (MPa)
(X)	0.783E8	415.402	75.6
(X/2)	0.105E9	415.431	113
(X/4)	0.137E9	415.444	168

It is also noted that the location with the maximum hydrostatic stress is different from where the current crowding occurs, from Figure 3 and Figure 4.

Unless further illustrated, all results reported in the following will be based on the mesh scheme of 'X/2'.

5. Negative Divergences of Atomic Fluxes

According to Equation 8, the divergences of atomic fluxes are the driving force for mass transport during current stressing. The divergences of the atomic fluxes due to electron wind, thermal gradient and hydrostatic stress gradient are calculated based on Equations 9 to 11 with a post processing script in our analysis.

First consider the case that the electrons flow through the corner ball from PCB to silicon chip. In this case, the electromigration is expected to occur at cathode on PCB side, as shown in Figure 5.

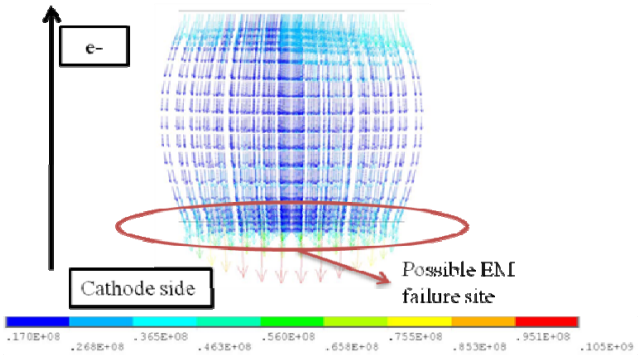

Figure 5 The current density vector plot when the current flows from chip to PCB side, i.e., electrons flows from PCB to chip side.

Since the maximum hydrostatic stress location is different from where the current crowding occurs, the divergences div $\vec{J}_{Em}$, div $\vec{J}_{Th}$ and div $\vec{J}_S$ are calculated for both locations, as given in Table 3. At the location where the maximum div $\vec{J}_{Em}$ is obtained, the div $\vec{J}_S$ is negative, which also results in a negative total divergence div $\vec{J}_{Tot}$. On the other hand, at the maximum hydrostatic stress location, all divergences are positive and result in a maximum total divergence. This would lead to a conclusion that the electromigration will occur at the location different from the current crowding location. This raises the question of the accuracy and validity of the formulation of the flux divergences by Equations 9 and 11.

Table 3 The Atomic Flux Divergence (atoms/m^3-s) Values Calculated at Max. Current Density and Max. Hydrostatic Stress Locations in the Bump when the Electrons Flow From PCB side to Chip side

Location	div J_{Tot}	div J_{Em}	div J_{Th}	div J_S
$\lvert\vec{J}\rvert$ max. location	-1.933e-5	1.00E-5	1.199E-7	-2.94E-5
σ_H max. location	1.39E-4	6.67E-6	2.69E-10	1.32E-4

Further, consider a second case in which the electrons flow through the corner ball from silicon chip to PCB, with the same magnitude of the current stressing (1.7A). In this case, the thermal and thermal-stress fields do not change. From Equation 2, the heat source resulted from joule heating will be same regardless of current flow direction. Therefore, temperature and thermal stress distribution remain same. However, the electromigration is expected to occur at the cathode near copper post of silicon chip side, as shown in Figure 6.

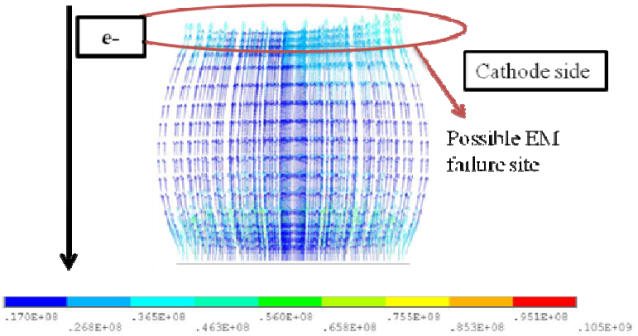

Figure 6 The current density vector plot when the current flows from PCB to chip side, i.e.,electrons flows from chip side to PCB side.

Therefore, the focus now is on the solder layer near copper post. Figure 7 plots the contours of the current density and hydrostatic stress of the top layer of the corner ball on silicon chip side. The maximum hydrostatic stress occurs at a location near or overlapping with current crowding location. Table 4 gives the values of the divergences of atomic fluxes for both locations. It turns out that a negative divergence due to electrical wind is obtained. This means even without considering thermo-mechanical stress induced migration, electromigration would not occur since the electron wind induced flux divergence is negative. These results are inconsistent with most of published test results on solder joints.

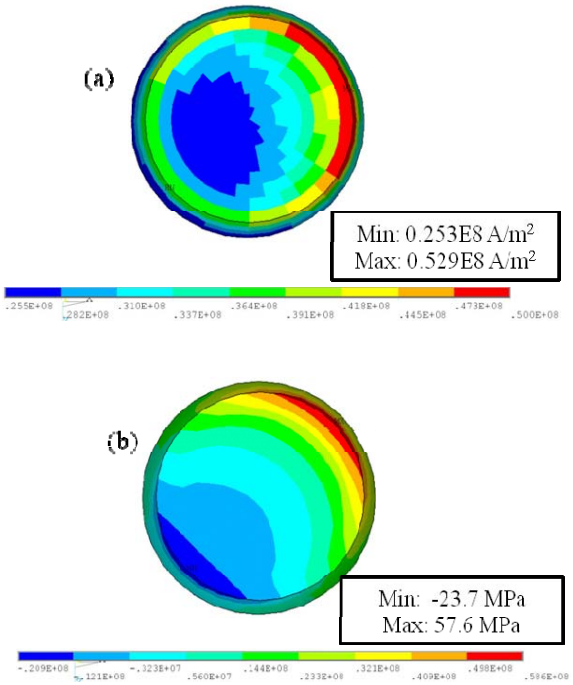

Figure 7 (a) Current density contour plot and **(b)** Hydrostatic stress contour plot on top layer of corner bump.

Table 4 The Atomic Flux Divergence (atoms/m^3-s) Values Calculated at Max. Current Density and Max. Hydrostatic Stress Locations in the Bump when the Electrons Flow From Chip side to PCB side

Location	div J_{Tot}	div J_{Em}	div J_{Th}	div J_S
$\|\vec{J}\|$ max. location	-1.0E-5	-5.97E-6	3.25E-8	-4.06E-6
σ_H max. location	-1.24-5	-5.55E-6	3.08E-8	-6.95E-6

In both cases, temperature fields are the same. It is also noted that the temperature gradient is very small in both cases, and the divergences due to thermal gradient is always positive but much less than the divergences due to current or thermal stresses (shown in Tables 3 & 4). However, such a small temperature gradient is necessary to keep the divergences of other components as non-zero, since according to the Equations 9 and 11, div $\vec{J}_{Em}$ and div $\vec{J}_s$ depend on the temperature gradient, as well.

From Equation (9), it can be seen that the sign of div $\vec{J}_{Em}$ depends on the dot product of $\vec{J}_{Em}$ and ∇T. When the current direction changes, the div $\vec{J}_{Em}$ will change from positive to negative since ∇T doesn't change. It is also noted that $\vec{J}_{Em}$ has opposite direction with respect to $\vec{J}$ since Z^* is a negative value.

The above results are obtained based on a copper post wafer level package. For a WLP with UBM structure [7], similar results are obtained. This means that a negative divergence due to electron current gradient at cathode near silicon chip is obtained when electrons pass bump from silicon to PCB. Such results are contradictory to the published test data.

6. Accuracy of Submodeling

To investigate the accuracy of submodeling used in this paper, a refined global finite element model with a mesh pattern exactly same to the submodel for the corner ball is examined. Figure 8(a) shows the current density distribution in the corner bump of the refined global model. The bump has a maximum current density of 0.106e9 A/m^2. Figure 8(b) shows the current density distribution from submodeling analysis. The bump has a maximum current density of 0.105e9 A/m^2. The current distribution plots for both models look exactly same.

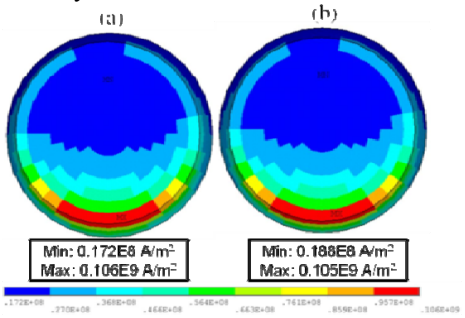

Figure 8 Current density distributions on the PCB side of corner bumps **(a)** Global model **(b)** Submodel

Figures 9(a) and 9(b) show the temperature distribution of the corner ball in the refined global model and submodel respectively. The results are almost identical. Figure 10(a) and 10(b) shows the hydrostatic stress distribution in the corner ball of the one refined global model, and submodel. The difference is negligible.

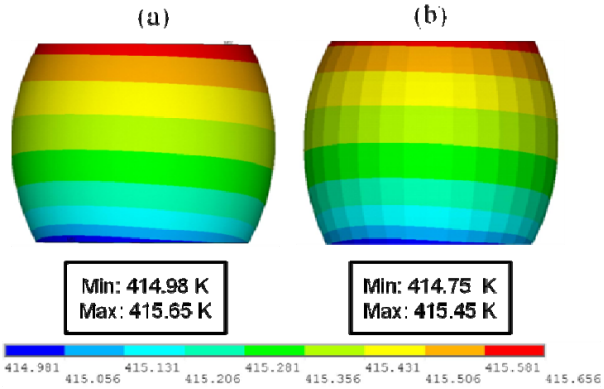

Figure 9 Temperature distributions in the corner bump **(a)** Global model **(b)** Submodel

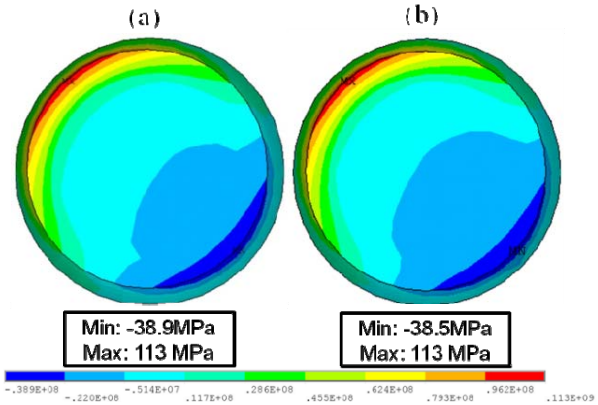

Figure 10 Hydrostatic stress distributions on the PCB side of corner bumps (a) Global model (b) Submodel

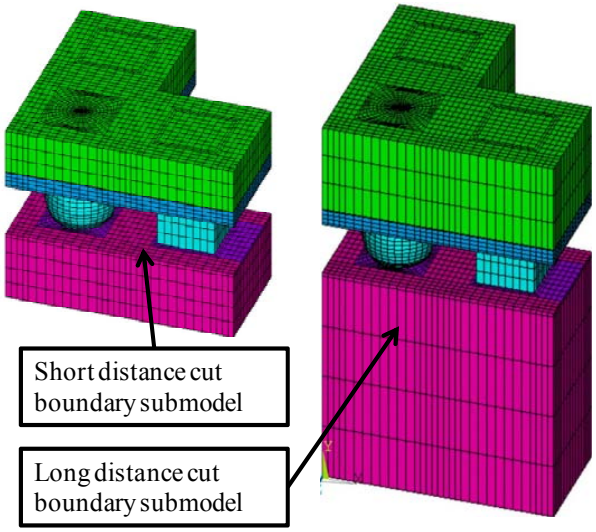

Figure 11 The two different cut boundary submodels considered for the analysis.

In the local model, care must be taken to select the cut boundary through PCB with a sufficient distance from the ball. Two cut distances are investigated (short distance and long distance cut boundary submodels as shown in Figure 11) and the results are given in Table 5. It is evident from the results that short distance cut boundary introduces significant errors.

Table 5 Cut Boundary Effect

$\lvert\vec{J}\rvert$ max. location	div J_{Tot}	div J_{Em}	div J_{Th}	div J_S
Long distance	-1.93E-5	1.0E-5	1.19E-7	-2.94E-5
Short distance	-1.6E-5	8.66E-6	1.21E-7	-2.47E-5
σ_H max. location	div J_{Tot}	div J_{Em}	div J_{Th}	div J_S
Long distance	1.39E-4	6.67E-6	2.69E-10	1.32E-4
Short distance	1.12E-4	5.41E-6	3.43E-9	1.07E-4

7. Conclusions

The finite element modeling of a directly coupled electrical-thermal-structural static analysis is performed to examine the electromigration in an encapsulated copper post wafer level package. Two finite element models, one global model and global/local (submodel) model, are designed for the analysis. Three different mesh schemes are examined in the submodel to investigate the singularity of current density. Results showed

1. The singularity of current density exists in bump structures. Both current density and hydrostatic stress exhibit a strong mesh-size dependency. However, temperature field has no singularity;
2. Based on the current mathematical formulations of the divergences of atomic fluxes due to electron wind gradient, thermal gradient and thermal stress gradient, negative divergences are obtained at cathode at the solder layer near silicon when electrons flow through the bump from silicon chip to PCB. Tan et al. [17] modified the driving force formulation, which does not affect the results presented here for the calculation of the divergence of atomic flux due to electron wind gradient. ∇N should be taken into consideration in the future study.
3. Submodeling produces accurate results compared to the refined global modeling results, with a great reduction in model size and computational time. The cut boundary must be taken far away from the location of the interest to eliminate the cut boundary effect.

References

[1]Ding, M., W. Guotao, C. Brook, and P. S. Ho. 2006, Effect of contact metallization on electromigration reliability of Pb-free solder joints. Journal of Applied Physics 99:094906

[2] Liu, P., Z. Wang, D. Chiang, M. Renavikar, B. Pathangey, R. Tanikella, C. Heath, and S. Ou, 2006. Electromigration failure mechanisms in P1264 SnPb and P1266 SnAg solder joints. Intel Assembly and Test Technology Journal 9: 473-482.

[3] Fan, X.J. and Liu, Y. 2009. Design, reliability and electromigration in chip scale wafer level packaging, Electronic Components and Technology Conference, Professional Development Short Course Notes.

[4] Tan, C. M., and A. Roy. 2006. Investigation of the effect of temperature and stress gradients on accelerated EM test for Cu narrow interconnects. Thin Solid Films 504: 288-293.

[5] Ye, H., C. Basaran, and D. Hopkins. 2003. Thermomigration in Pb-Sn solder joints under joint heating during electric current stressing. Applied Physics Letters 82: 1045-1047.

[6] Dalleau, D., and K. Weige-Zaage. 2001. Three-dimensional voids simulation in chip-level metallization structures: A contribution to reliability evaluation. Microelectronic Reliability 41: 1625-30.

[7] Liu, Y., L. Liang, S. Irving, and T. Luk. 2008. 3D modeling of electromigration combined with thermal-mechanical effect for IC device and package. Microelectronics Reliability 48: 881-824.

[8] Fan, X. J., H. B. Wang, and T. B. Lim. 2001. Investigation of the underfill delamination and cracking in flip-chip modules under temperature cyclic loading. IEEE Transactions on Components and Packaging Technologies 24: 84-91

[9] Dandu, P., X. J. Fan, Y. Liu, and C. Diao. 2010. Finite element modeling on electromigration of solder joints in wafer level packaging. Microelectronic Reliability: doi:10.1016/j.microrel.2009.12.003.

[10] Choi, W. J., E. C. C. Yeh, and K. N. Tu. 2002. Electromigration of flip chip solder joints on Cu/Ni(V)/AI thin film under bump metallization. Electronic Components and Technology Conference, May 28-31, San Diego, CA.

[11] Liang, L.H., and Y. Liu. 2006. Reliability study in solder joint under electromigration thermal–mechanical load. International Conference on Electronics Packaging Technology, August, Shanghai, China.

[12] Liang, S.W., T. L. Shao, and C. Chen. 2005. 3-D simulation on current density distribution in flip-chip solder joints with thick Cu UBM under current stressing. Electronic Components and Technology Conference, May 31-June 3, Florida, USA.

[13] Nah, J.W., Fei Ren, and K. N. Tu. 2006. Electro migration in Pb-free flip chip solder joints on flexible substrates. Applied Physics Letter 99: 023520.

[14] Lai, Y. S., K. M. Chen, and C. L. Kao. 2006. Electromigration of Sn–37Pb and Sn–3Ag– 1.5Cu/Sn–3Ag–0.5Cu composite flip-chip solder bumps with Ti/Ni(V)/Cu under bump metallurgy. Microelectronic Reliability 48: 811-824.

[15] Yue, H., C. Basaran, D. Hopkins, and M. Lin. 2005. Modeling deformation in microelectronics BGA solder joints under high current density, part I: simulation and testing. Electronic Components and Technology Conference, May 27-30, New Orleans, LA.

[16] Gee, Steve, N. Kelkar, Joanne Huang, and K. N. Tu. 2005. Leed-free and PbSn bump electromigration testing. ASME Inter PACK, July 17-22, San Francisco, CA.

[17] Tan, C.M., Y. Hou, and W. Li. 2007. Revisit to the finite element modeling of electromigration for narrow interconnects. Journal of Applied Physics 102: 033705.